Highly Spin-Polarized Conducting State at the Interface between Nonmagnetic Band Insulators: $LaAlO_3/FeS_2$ (001)

J. D. Burton* and E. Y. Tsymbal†

Department of Physics and Astronomy, Nebraska Center for Materials and Nanoscience, University of Nebraska, Lincoln, Nebraska 68588-0299, USA

(Received 29 June 2011; published 11 October 2011)

First-principles density functional calculations demonstrate that a spin-polarized two-dimensional conducting state can be realized at the interface between two nonmagnetic band insulators. The (001) surface of the diamagnetic insulator FeS_2 (pyrite) supports a localized surface state deriving from Fe d orbitals near the conduction band minimum. The deposition of a few unit cells of the polar perovskite oxide $LaAlO_3$ leads to electron transfer into these surface bands, thereby creating a conducting interface. The occupation of these narrow bands leads to an exchange splitting between the spin subbands, yielding a highly spin-polarized conducting state distinct from the rest of the nonmagnetic, insulating bulk. Such an interface presents intriguing possibilities for spintronics applications.

DOI: 10.1103/PhysRevLett.107.166601 PACS numbers: 72.25.Mk, 73.20.At, 73.40.−c

With the ever approaching scaling and power consumption limit of current semiconductor device technology, the search is on for new materials systems which could form the basis of the next of generation of devices [1]. Going beyond traditional semiconductors to other materials, such as complex oxides [2] and transition metal sulfides [3,4], could lead to lower power consumption and better scalability by offering more functionality based on various magnetic and electric degrees of freedom [5]. This is especially true for atomically engineered interfaces where properties can be found that even the bulk constituents do not possess [6].

One prominent system is the two-dimensional electron gas (2DEG) formed at the (001) interface between two insulating perovskite oxides, $LaAlO_3$ and $SrTiO_3$ [7]. Because $LaAlO_3$ consists of atomic planes of alternating charge, charge is transferred to the interface to eliminate the internal electric field, leading to a 2DEG above a certain critical thickness of $LaAlO_3$ [8,9]. Tunable metallic properties of this interface are promising for potential applications [10–14]. In addition, magnetism [15] and superconductivity [16] have been discovered at this interface, suggesting further implications for nanoelectronics [6].

A spin-polarized 2DEG is an exciting prospect for spintronics, where involvement of the spin degree of freedom broadens the spectrum of potential applications [17]. Several systems have been proposed to incorporate magnetism, e.g., replacing $LaAlO_3$ with the strongly correlated oxide $LaVO_3$ [18], embedding a LaO monolayer in $SrMnO_3$ [19], and exploiting the ferromagnetism of EuO [20,21]. These interfaces inherit magnetic properties from the constituent materials, either through magnetic order or their tendency toward strong correlations.

We propose a different approach to create a spin-polarized 2DEG: magnetism is induced at the interface between two nonmagnetic insulators due to charge-transfer-driven exchange splitting of the interface states. Such an interface can be realized by pairing $LaAlO_3$ with the diamagnetic band insulator FeS_2, commonly known as pyrite. FeS_2 begins a series of pyrite-structure disulfides covering the late half of the $3d$ elements all the way to ZnS_2, each displaying properties distinct from its neighbors [22]. In particular, CoS_2 has one more d electron per formula unit than FeS_2, making it an itinerant ferromagnetic metal. Changing this charge through alloying of CoS_2 and FeS_2 allows tuning of the magnetic and transport properties [3,23]. This suggests that by electron doping of a pure FeS_2 surface through heterostructuring with polar $LaAlO_3$ both conductivity and magnetism might exist at the same interface.

Here we present results of first-principles density functional theory (DFT) calculations of $LaAlO_3/FeS_2$ (001) interfaces that confirm the conducting and ferromagnetic behaviors at this interface. These properties are confined to the interface due to native surface states of FeS_2 which are susceptible to Stoner exchange splitting when occupied, leading to itinerant ferromagnetism and substantial spin polarization.

DFT calculations are performed using the plane-wave pseudopotential method implemented in the QUANTUM ESPRESSO package [24]. A plane-wave cutoff energy of 400 eV and a generalized-gradient approximation [25] were used in all calculations. Atomic relaxations were converged using a $4 \times 4 \times 1$ Monkhorst-Pack $\boldsymbol{k}$-point mesh, Gaussian broadening of 0.1 eV, and force cutoff of 20 meV/Å. The resulting structures were used in subsequent frozen-lattice self-consistent calculations using a $10 \times 10 \times 1$ $\boldsymbol{k}$-point mesh and broadening of 0.02 eV to refine the electronic density. Subsequent non-self-consistent calculations on a $48 \times 48 \times 1$ $\boldsymbol{k}$-point mesh were performed to extract $\boldsymbol{k}_{\parallel}$-resolved local density of states (LDOS) with 7 meV broadening.

 © 2011 American Physical Society

Bulk FeS_2 has a quasirocksalt cubic structure consisting of Fe^{2+} at the face centers and $S_2{}^{2-}$ dimers centered at the cube corners alternately aligned along the various body-diagonal axes, resulting in space group $Pa\bar{3}$. Calculations yield a cubic lattice constant of $a = 5.410$ Å and a $S_2{}^{2-}$ bond length of $d = 2.194$ Å, in agreement with previous calculations [26–28] and experiments [29].

We study three heterostructure systems, shown in Fig. 1. In all cases the in-plane lattice parameter is fixed to that calculated for bulk FeS_2 to mimic epitaxial growth on a single crystal or well-relaxed film. The vertical supercell size is $13a = 70.33$ Å. First we study the slab consisting of 5 stoichiometric (001) layers of FeS_2 embedded in vacuum [see Fig. 1(a)] [30]. Other surface terminations are energetically unfavorable, making (001) an ideal cleavage plane for single crystals resulting in flat, atomically stepped, terraces up to a few hundred nm wide [31]. Atomic relaxation does not introduce dramatic changes to the structure with respect to the bulk, consistent with previous calculations [32,33] and experimental data [31,34].

In bulk, Fe^{2+} cations are sixfold coordinated by sulfur. The crystal field splits the $3d$ manifold into a low-lying t_{2g} triplet and a higher energy e_g doublet. This splitting is large enough that the zero-spin state is favored with 6 electrons in the t_{2g} orbitals, leaving the e_g orbitals above the highly dispersive S $3p$ states that form the conduction band minimum. This is evident from the LDOS of the bulk FeS_2 layer in Fig. 2(a). On the (001) surface Fe^{2+} cations are only fivefold coordinated, modifying the crystal field environment of the Fe $3d$ states. The e_g doublet is split and the t_{2g} states are split into a low singlet and a higher doublet. These split levels alone do not close the gap, leaving 6 spin-paired electrons in the "t_{2g}" sector of the manifold. Since this change in splitting is localized at the surface, however, the high-lying levels of the t_{2g} triplet and the low-lying member of the "e_g" doublet constitute surface states near the top of the valence band and the bottom of the conduction band, respectively.

These surface states are seen in Fig. 2(a) as peaks at around $E_F \pm 0.4$ in the LDOS on FeS_2-1 which are not present in the bulk DOS, but quickly decay into the subsurface layers. (For gapped systems the Fermi level E_F is at the center of the band gap.) The decay of the conduction band surface states is also seen in the $\boldsymbol{k}_{\parallel}$ and layer-resolved LDOS plotted in Figs. 3(a)–3(c) at $E_F + 0.4$ eV. The narrow energy contours correspond to cuts through a two-dimensional band structure, demonstrating a decrease in intensity when moving from the surface [Fig. 3(a)] to the bulk [Fig. 3(c)]. The circles around the Γ point correspond to cuts through the dispersive S $3p$ states.

Next we study the $LaAlO_3/FeS_2$ (001) interface. Bulk $LaAlO_3$ deviates from the perfect cubic perovskite structure by tilts and rotations of the oxygen octahedra around the Al sites, resulting in space group $R\bar{3}c$. Our generalized-gradient approximation calculations of the bulk $R\bar{3}c$ structure reveal a volume consistent with a cubic perovskite lattice parameter $a_{cp} = 3.817$ Å. Epitaxial matching with the pyrite structure requires a $\sqrt{2} \times \sqrt{2}$ in-plane doubling of the pseudocubic perovskite cell with a 45° rotation around the pseudocubic [001] direction,

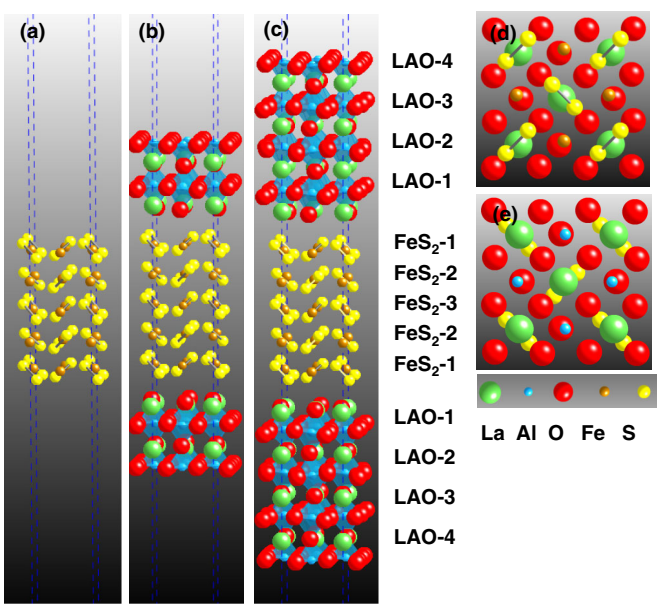

FIG. 1 (color online). Atomic structures of the three systems studied: (a) FeS_2 slab consisting of five (001) atomic layers; (b), (c) symmetric heterostructures with the FeS_2 slab covered by (b) 2 and (c) 4 u.c. $LaAlO_3$ films; (d) bottom and (e) top views of the first few monolayers near the interface.

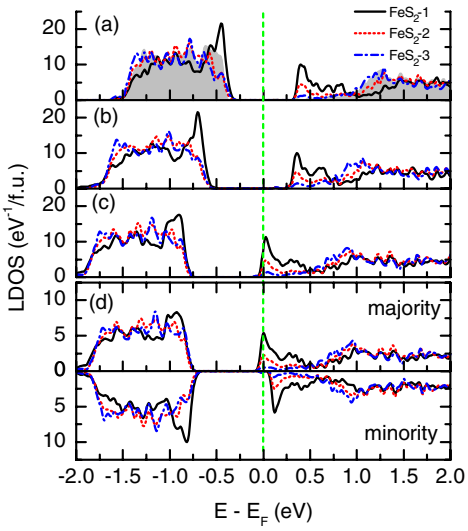

FIG. 2 (color online). LDOS projected onto layers FeS_2-1 through FeS_2-3 (see Fig. 1) for a FeS_2 slab surrounded by (a) vacuum, (b) 2 u.c. $LaAlO_3$, and (c),(d) 4 u.c. $LaAlO_3$, as follows from non-spin-polarized (c) and spin-polarized (d) calculations. The vertical dashed line indicates E_F. In (a) the filled curve is the total DOS of bulk FeS_2.

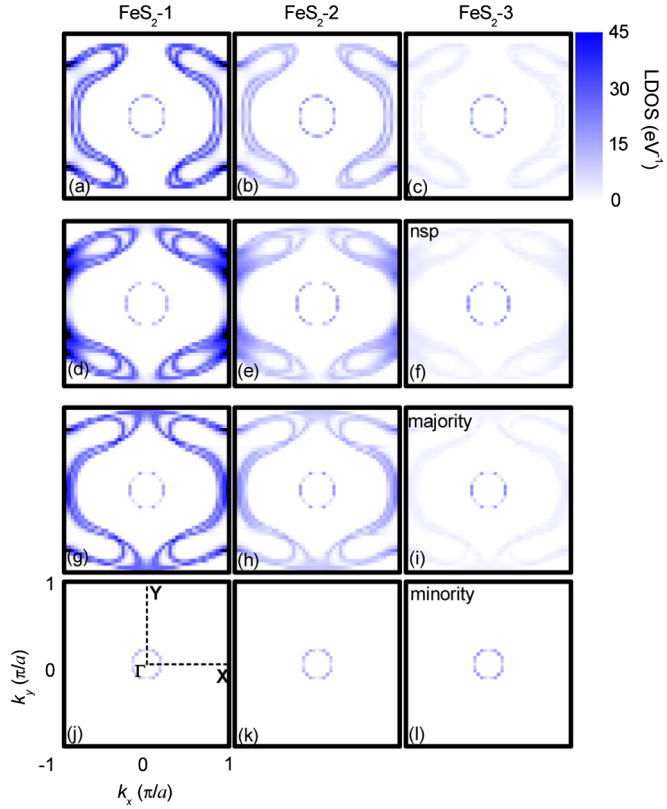

FIG. 3 (color online). $\boldsymbol{k}_{\parallel}$-resolved LDOS projected onto layers FeS_2-1 through -3 (see Fig. 1) for a FeS_2 slab, $E = E_F + 0.4$ eV (a)–(c) and $LaAlO_3$(4 u.c.)/FeS_2 heterostructure, $E = E_F$ (d)–(l). Results of non-spin-polarized (d)–(f) and spin-polarized calculations for majority (g)–(i) and minority-spin (j)–(l) are shown.

leading to an effective in-plane lattice constant of $\sqrt{2}a_{cp} = 5.398$ Å. Matching to the FeS_2 lattice leads to -0.2% tensile strain, and calculations of bulk $LaAlO_3$ for this strain state reveal a $C2/c$ structure, consistent with previous calculations [35].

Using this $C2/c$ structure we construct the heterostructures by adding 2 unit cell (u.c.) and 4 u.c. $LaAlO_3$ layers to the FeS_2 slab, as shown in Figs. 1(b) and 1(c), respectively. $LaAlO_3$ films are stoichiometric with LaO termination at the interface with FeS_2 and AlO_2 termination with vacuum. The LaO interface termination, with La^{3+} above the center of the S_2^{2-} dimers and O^{2-} above the Fe^{2+} sites, is a natural extension of the quasirocksalt ionic structure of the FeS_2 surface [Figs. 1(d) and 1(e)]. Each supercell is inversion symmetric, eliminating any electric field in the vacuum regions. Supercells are sufficiently large to minimize interactions across the vacuum. The structures are then fully relaxed, resulting in layer-by-layer polar distortions (see Fig. S1 in the Supplemental Material [36]) due to internal electric fields as was found for similar systems [9].

The 2 u.c. $LaAlO_3$ system maintains a small, but true, band gap and thus remains insulating. Nevertheless, since

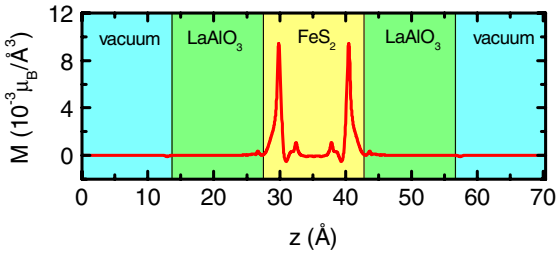

FIG. 4 (color online). Distribution of magnetization M in the 4 u.c. heterostructure averaged over the plane parallel to the layers.

the electric field in the $LaAlO_3$ has decreased the overall band gap, the states at the bottom of the conduction band of FeS_2 are closer to E_F than those for the FeS_2 slab [Fig. 2(a)]. (See also Fig. S2a in the Supplemental Material [36].) This tendency persists with increasing $LaAlO_3$ thickness, and for the 4 u.c. $LaAlO_3$ heterostructure we find the overall band gap has closed, leaving E_F within the conduction band of FeS_2, thus indicating metallicity of the interface [see Fig. 2(c)]. (See also Fig. S2b in the Supplemental Material [36].) This behavior is consistent with the charge transfer mechanism known for the well-studied $LaAlO_3/SrTiO_3$ system [9,37,38]. The charge transfer amounts to $\sim$0.16 electrons/interface Fe. This is consistent with the $LaAlO_3/SrTiO_3$ system where, above a critical thickness of $LaAlO_3$, electron transfer approaches 0.5 electrons in the limit of large $LaAlO_3$ thickness [38].

The transferred electrons are almost entirely accommodated into the localized FeS_2 interface states. This is seen from the $\boldsymbol{k}_{\parallel}$-resolved LDOS plotted in Figs. 3(d)–3(f), where the narrow contours correspond to the Fermi surface of this conducting interface, which are similar to the bare surface states in Figs. 3(a)–3(c).

The above calculations assumed no spin polarization. This constraint results in a large peak in the non-spin-polarized LDOS at E_F on the interface in the 4 u.c. $LaAlO_3$ heterostructure [Fig. 3(c)]. This suggests that exchange splitting of the spin bands might reduce electron energy [39,40], and spin-polarized calculations confirm this prediction. Figure 4 shows the spin density profile revealing that the magnetic moment comes mostly from the Fe sites in the FeS_2-1 layer, whereas the magnetization in the rest of the structure is negligible. The induced moment is $0.13\mu_B$ per interface Fe, which is remarkably consistent with what is found experimentally for bulk $Fe_{1-x}Co_xS_2$ with $x = 0.16$ [22], corresponding to the charge transfer of $0.16e$ found in our interface calculations. Spin-polarized calculations for the FeS_2-vacuum slab and the heterostructure with 2 u.c. of $LaAlO_3$, however, do not reveal any magnetization, consistent with zero charge transfer.

As seen from Fig. 2(d), the exchange splitting of the interface states is 0.11 eV. This completely splits the Fe d states, making the system nearly half-metallic with

Fermi-level LDOS dominated by the majority-spin states. The spin- and $\boldsymbol{k}_{\parallel}$-resolved LDOS in FeS_2 are plotted in Figs. 3(g)–3(l). The majority-spin LDOS [Figs. 3(g)–3(i)] looks similar to those for the non-spin-polarized interface states. The minority-spin LDOS [Figs. 3(j)–3(l)] displays only a two-dimensional electron pocket, corresponding to the dispersive S $3p$ states.

The appearance of exchange splitting of the interface states is consistent with the Stoner model for itinerant ferromagnetism [39]. This model begins with the nonmagnetic DOS, $\rho(\varepsilon)$, and transfers electrons from minority- to majority-spin states giving rise to a magnetic moment m. Lowering in energy occurs due to the reduced Coulomb interaction, characterized by the parameter I, between electrons occupying the same orbital. This competes with an increase in the overall kinetic, or "band," energy of the system. If the condition $I\rho(\varepsilon_F) > 1$ is satisfied, then a stable magnetic moment is present, given by the relation $\Delta = Im$, where Δ is the exchange splitting between spin bands. Taking $m = 0.13\mu_B/\mathrm{Fe}$ and $\Delta = 0.11$ eV from the LDOS in Fig. 2(d), we find an exchange parameter $I = 0.84$ eV. This is consistent with first-principles calculations of I discussed in the Supplemental Material [36], as well as previous calculations [41] and values derived from experiments for Fe-containing systems [42]. In addition, previous DFT calculations of bulk $(\mathrm{Fe, Co})S_2$ alloys also reproduce quite well experimental trends of magnetic moment [3]. These facts indicate that our results do not suffer from incomplete account of electron correlations.

In conclusion, we have predicted a conducting ferromagnetic interface between two nonmagnetic band insulators, $LaAlO_3$ and FeS_2. The polar nature of the $LaAlO_3$ (001) layer supports charge transfer to a localized interface state formed by Fe d orbitals at the conduction band minimum of FeS_2. This nearly half-metallic interface may be interesting for spintronics applications.

This work was supported by the National Science Foundation (Grants Nos. DMR-0906443 and No. EPS-1010674). Computations were performed utilizing the Holland Computing Center of the University of Nebraska.

*jdburton1@gmail.com
†tsymbal@unl.edu

[1] http://www.itrs.net/Links/2010ITRS/Home2010.htm
[2] Y. Tokura and H. Y. Hwang, Nature Mater. **7**, 694 (2008).
[3] I. I. Mazin, Appl. Phys. Lett. **77**, 3000 (2000).
[4] L. Wang *et al.*, Phys. Rev. Lett. **94**, 056602 (2005).
[5] J. P. Velev *et al.*, Surf. Sci. Rep. **63**, 400 (2008).
[6] J. Mannhart and D. G. Schlom, Science **327**, 1607 (2010).
[7] A. Ohtomo and H. Y. Hwang, Nature (London) **427**, 423 (2004).
[8] N. Nakagawa, H. Y. Hwang, and D. A. Muller, Nature Mater. **5**, 204 (2006).
[9] R. Pentcheva and W. E. Pickett, Phys. Rev. Lett. **102**, 107602 (2009).
[10] S. Thiel *et al.*, Science **313**, 1942 (2006).
[11] C. Cen *et al.*, Science **323**, 1026 (2009).
[12] M. K. Niranjan *et al.*, Phys. Rev. Lett. **103**, 016804 (2009).
[13] C. W. Bark *et al.*, Proc. Natl. Acad. Sci. U.S.A. **108**, 4720 (2011).
[14] H. W. Jang *et al.*, Science **331**, 886 (2011).
[15] A. Brinkman *et al.*, Nature Mater. **6**, 493 (2007).
[16] N. Reyren *et al.*, Science **317**, 1196 (2007).
[17] I. Zutic, J. Fabian, and S. D. Sarma, Rev. Mod. Phys. **76**, 323 (2004).
[18] Y. Hotta, T. Susaki, and H. Y. Hwang, Phys. Rev. Lett. **99**, 236805 (2007).
[19] B. R. K. Nanda and S. Satpathy, Phys. Rev. Lett. **101**, 127201 (2008).
[20] Y. Wang *et al.*, Phys. Rev. B **79**, 212408 (2009).
[21] J. Lee, N. Sai, and A. A. Demkov, Phys. Rev. B **82**, 235305 (2010).
[22] H. S. Jarrett *et al.*, Phys. Rev. Lett. **21**, 617 (1968).
[23] L. Wang *et al.*, Phys. Rev. B **73**, 144402 (2006).
[24] P. Giannozzi *et al.*, J. Phys. Condens. Matter **21**, 395502 (2009).
[25] J. P. Perdew, K. Burke, and M. Ernzerhof, Phys. Rev. Lett. **77**, 3865 (1996).
[26] V. Eyert *et al.*, Phys. Rev. B **57**, 6350 (1998).
[27] I. Opahle, K. Koepernik, and H. Eschrig, Phys. Rev. B **60**, 14 035 (1999).
[28] J. Muscat *et al.*, Phys. Rev. B **65**, 054107 (2002).
[29] S. L. Finklea, III, L. Cathey, and E. L. Amma, Acta Crystallogr. Sect. A **32**, 529 (1976).
[30] Calculations of a 9 layer pyrite slab embedded in vacuum exhibit essentially identical surface relaxation and electronic structure.
[31] K. M. Rosso, U. Becker, and M. F. Hochella, Am. Mineral. **84**, 1535 (1999).
[32] A. Hung *et al.*, Surf. Sci. **513**, 511 (2002).
[33] A. Stirling, M. Bernasconi, and M. Parrinello, J. Chem. Phys. **118**, 8917 (2003).
[34] K. M. Rosso, Rev. Mineral. Geochem. **42**, 199 (2001).
[35] A. J. Hatt and N. A. Spaldin, Phys. Rev. B **82**, 195402 (2010).
[36] See Supplemental Material at http://link.aps.org/supplemental/10.1103/PhysRevLett.107.166601 for atomic displacements of all three structures, electronic LDOS of $LaAlO_3$, and a description of the Stoner modeling.
[37] J. Lee and A. A. Demkov, Phys. Rev. B **78**, 193104 (2008).
[38] H. Chen, A. Kolpak, and S. Ismail-Beigi, Phys. Rev. B **82**, 085430 (2010).
[39] E. C. Stoner, Proc. R. Soc. A **165**, 372 (1938).
[40] K. Janicka, J. P. Velev, and E. Y. Tsymbal, J. Appl. Phys. **103**, 07B508 (2008).
[41] P. M. Marcus and V. L. Moruzzi, Phys. Rev. B **38**, 6949 (1988).
[42] O. Gunnarsson, J. Phys. F **6**, 587 (1976).